

# Simulation of Airlift Pumps for Deep Water Wells

A. NENES<sup>1</sup>, D. ASSIMACOPOULOS<sup>1</sup>, N. MARKATOS<sup>1</sup>, and E. MITSOULIS<sup>2\*</sup>

<sup>1</sup>*Department of Chemical Engineering, National Technical University of Athens,*

*GR-157 80 Athens, Greece*

<sup>2</sup>*Department of Chemical Engineering, University of Ottawa,*

*Ottawa, Ontario K1N 6N5, Canada*

\* Author to whom correspondence should be addressed

**Abstract**

A mathematical model for the simulation of water airlift pumps is developed, based on the "interspersed continua" approximation for two-phase flow systems, together with an algorithm that selects the appropriate friction correlation for specific flow regimes. The model presented can either predict the water or air flow rate for a given airlift system. Predictions obtained by the model were compared with a series of experiments performed by the Greek Institute of Geological and Mineral Exploration and were found to be in good agreement. The present predictions are far superior to those obtained by an existing simple model currently in general use.

Keywords: airlift pumping, two-phase flow, flow regime prediction, finite-volume method

## Introduction

Airlift pumping was invented by Carl Loscher at the end of the eighteenth century (Giot, 1982). Operation is based on the pumping effect achieved when air is injected into a liquid or a solid-liquid mixture. This type of pumping system has a low efficiency in comparison with other pumping methods. However, simplicity in construction and absence of moving mechanical parts are two very important advantages that make it useful in certain applications, such as pumping corrosive liquids (sandy or salty waters) (Giot, 1982) and viscous liquids (e.g., hydrocarbons in the oil industry) (Giot, 1982; Kato et al., 1975). Airlift pumping is also used in shaft and well drilling (Giot, 1982; Gibson, 1961) (the drillings being lifted by underground water), undersea mining (Giot, 1982; Mero, 1968), and in certain bioreactors and waste-treatment installations, providing excellent aeration of the pumped fluid (Chisti, 1992; Tristram et al., 1992).

A typical airlift pump involves a vertical pipe of length  $L$  divided into two parts (Figure 1). A *suction pipe* of length  $L_e$  between the bottom end and the air injection port (points 1 and i), and an *upriser pipe* of length  $L_u$  between the air and discharge ports (points i and 2), which is partially submerged by a length  $L_s$ .

The type of flow in the suction pipe is either one-phase (liquid) or two-phase (solid-liquid) while in the upriser pipe is either two-phase (air-liquid) or three-phase (air-liquid-solid). The upriser pipe can be of constant or varying diameter, increasing from injection to discharge point (tapered systems). The latter are much more efficient when pumping from large depths, because this ensures slug flow along the upriser. Otherwise, i.e., when a fixed diameter system is used, due to gas expansion, the flow changes to annular, which is characterized by poor pumping efficiency (Giot, 1982).

Air supplied from a compressor is injected through an external or internal airline (Figure 2). At the beginning of pump operation, an initial drop in water level is observed, depending on the rate of pumping. There is also an additional drop in water level during pump operation, but it is usually very small and for simplicity omitted. Thus, two water levels are defined, one at *idling conditions*, and one during *pump operation*. The first level determines the compressor hydraulic overhead, i.e., the pressure in which the compressor must initially supply air for the pump to start operating. The second level affects operation parameters (water outflow, submergence, etc.), and determines the pressure at which the pump must supply air during steady-state conditions.

Although external airline systems are more efficient, internal airline pumps are more frequently used because of their versatility and ease in assembly. As the water level inside the well fluctuates or changes, maximum efficiency can always be achieved by changing the airline length inside the upriser.

Simulation of the pump is essential for determining the optimum operational conditions. For this purpose, various correlations (Zenz, 1993) and simple mathematical models (Kato et al., 1975; Casey, 1992) have been proposed. This paper presents a *new model* for the pumping of a liquid (water) and uses a more sophisticated approach to simulate the flow of the two-phase mixture in the upriser part. The model uses the full differential equations describing two-phase flows, that are based on the well-established *interspersed continua* concept. Finite-volume techniques together with the interphase-slip algorithm (IPSA) (Markatos and Singhal, 1982) are used for solving the system of differential equations. Friction terms in the momentum equations are calculated by correlations appropriate for various types of flow regimes. A flow regime map (Taitel et al., 1980) predicts the flow pattern at any point in the pumping system, using the local flow rate and physical properties of air and water. The model can give predictions, among others, for important design parameters such as the liquid outflow rate for a given type of compressor,

and the air flow rate needed to achieve a certain liquid flow rate from the well (i.e., air compressor specifications).

Furthermore, the present work includes analysis of real field data collected from experiments on the outflow rate of the airlift pump. The experimental results have been compared with predictions given by the new model and by another one currently in general use.

## **Mathematical modelling**

Kato et al. (1975) proposed a simple model for airlift simulation, based on the momentum balance along the upriser and the use of a mean air-volume fraction (see appendix for a detailed reference of working equations). *The mean air-volume fraction model* is valid for both internal and external airline systems, and a simplified version for external airline systems is given by Giot (1982). The model, although simple in use, has two major drawbacks: (i) predictions are acceptable for wells up to 11 meters deep, due to the assumption of a single flow regime along the upriser (slug flow), and (ii) the model is heavily dependent on empirical information (correlations) needed for air-volume fraction and friction drop calculations.

In the present work, the simulation of the air-lift pump is carried out through a full *hydrodynamic model* solved numerically using iterative procedures. The low accuracy of the mean air-volume fraction model mentioned above can be improved by describing the flow along the upriser with a standard set of differential equations, suitable for two-phase flows. Empirical correlations are used only for calculating the friction terms, while the possibility of many flow regimes is also allowed, the type of which is determined by a flow regime map. The differential equations are integrated and solved by using the finite-volume method. Flow in the suction pipe is calculated by simply applying the Bernoulli equation and inserting an additional term for friction in the entry region of the suction pipe.

The analysis takes place in two steps, one for the suction pipe and another for the upriser. The pressure at the injection point is calculated independently in these two steps. A physically acceptable solution is obtained when these pressures are equal, and this represents the convergence criterion of the model.

#### A. Flow in the suction pipe

The flow in the suction pipe is simulated by applying the Bernoulli equation between points 1 and i (see Figure 1):

$$P_i = P_1 - \rho_l g L_e + \left( \frac{dP}{dz} \right)_{f,l} L_e \quad (1)$$

The pressure at point 1 is calculated according to the following formula, provided the water level during operation is known:

$$P_1 = P_2 + \rho_l g (L_s + L_e) - \xi \frac{M_l^2}{2 \rho_l A_1^2} \quad (2)$$

where  $\xi$  is the pipe entry loss factor and is approximately equal to 0.5. The friction pressure drop is calculated by the following relations:

$$\left( \frac{dP}{dz} \right)_{f,l} = -f_m \frac{4}{D_1} \frac{M_l^2}{2 \rho_l A_1^2} \quad (3)$$

$$f_m = \begin{cases} 16 / \text{Re}_l & \text{when } \text{Re}_l \leq 2000 \\ 0.079 \text{Re}_l^{-0.25} & \text{when } \text{Re}_l > 2000 \end{cases} \quad (4)$$

$$\text{Re}_l = \frac{M_l D_1}{A_1 \mu_l} \quad (5)$$

### *B. Flow in the upriser*

The governing equations are derived from application of mass and momentum conservation principles over differential control volumes. The approach is based on the space-sharing *interspersed-continua* concept (Markatos, 1986), according to which the two phases share the space, and each phase can occupy a certain point in space with a probability expressed by its *volume fraction*,  $R$ . The following assumptions have been made in formulating the equations:

- steady-state operating conditions;
- compressible gas phase;
- no exchange of mass between phases;
- exchange of momentum between phases only through interphase friction processes;
- isothermal flow for both phases;
- one common pressure field for both phases; and
- one-dimensional variation of properties within a cylindrical co-ordinate system with the variation axis defined along the upriser.

The independent variable is the distance measured from the injection port  $z$  (Figure 3). Although a steady-state flow is assumed, the unsteady set of equations (Markatos and Singhal, 1982; Markatos, 1986) is used, as the transient solution of the differential equations increases the stability and convergence of the algorithm.

#### *Continuity*

For the gaseous phase:

$$\frac{\partial R_g}{\partial t} + \frac{\partial}{\partial z}(R_g U_g) = -\frac{R_g}{\rho_g} \left[ \frac{\partial \rho_g}{\partial t} + U_g \frac{\partial \rho_g}{\partial z} \right] \quad (6)$$

For the liquid phase:

$$\frac{\partial R_l}{\partial t} + \frac{\partial}{\partial z}(R_l U_l) = 0 \quad (7)$$

*Momentum conservation*

For the gaseous phase:

$$\frac{\partial}{\partial t}(R_g \rho_g U_g) + \frac{\partial}{\partial z}(R_g \rho_g U_g^2) = -R_g \frac{\partial P}{\partial z} + f_z^{gl} + f_z^{gw} - R_g \rho_g g \quad (8)$$

where  $f^{gl}$  and  $f^{gw}$  are the gas-liquid and gas-wall friction terms, respectively.

For the liquid phase:

$$\frac{\partial}{\partial t}(R_l \rho_l U_l) + \frac{\partial}{\partial z}(R_l \rho_l U_l^2) = -R_l \frac{\partial P}{\partial z} + f_z^{lg} + f_z^{lw} - R_l \rho_l g \quad (9)$$

where  $f^{lg}$  and  $f^{lw}$  are the liquid-gas and liquid-wall friction terms, respectively. The interphase friction source terms  $f^{lg}$  and  $f^{gl}$  always satisfy the following relation:

$$f^{lg} = -f^{gl} \quad (10)$$

The volume fractions at every point must satisfy the constraint (also known as *consistency criterion*):

$$R_g + R_l = 1 \quad (11)$$

i.e., the space is fully occupied by the two phases.

The perfect gas law was used for calculating the air density.

The solution of the governing equations is possible after a complete set of boundary conditions has been defined. At the injection port  $i$ , the following boundary conditions are prescribed:

$$R_l = 1.0 \quad R_g = 0 \quad (12)$$

$$U_l = \frac{M_l}{R_l \rho_l A_2}$$

At the discharge point 2, the pressure  $P_2$  is known (atmospheric conditions), and a free outflow boundary condition is implied on the remaining four variables  $R_g, R_b, U_g, U_l$ :

$$\frac{\partial R_g}{\partial z} = \frac{\partial R_l}{\partial z} = \frac{\partial U_g}{\partial z} = \frac{\partial U_l}{\partial z} = 0 \quad (13)$$

### *C. Flow regimes and friction correlations*

Interphase friction is calculated from correlations that differ within each flow regime. In order to select the appropriate relation for each cell, a flow map proposed by Taitel et al. (1980) is employed. This map uses phase velocity, volume fraction, density and pipe position in order to predict the type of flow regime prevailing. During the solution this procedure of the finite-volume equations is repeated for every cell and allows the prediction of different local flow regimes and physical properties along the upriser. A typical map is shown in Figure 4.

Change in flow regime results in *jumps* in the interphase friction factor, which may lead to convergence problems. In order to smooth discontinuities and ensure good numerical behaviour, transition regions between regimes are used (instead of transition lines), in which friction coefficients are calculated as a weighted mean of the correlations used for both regimes.

The *wall-phase frictional forces* integrated over the volume of the computational cell for phase  $i$  are calculated from the relation (Markatos and Singhal, 1982):

$$F_{iw} = \int f^{iw} dV_p = 0.5 f_{iw} \rho_i U_i^2 A_{iw} \quad (14)$$

where  $V_p$  is the volume of the computational cell,  $f^{iw}$  is the volumetric friction force term given in the momentum equation,  $f_{iw}$  is the friction coefficient,  $\rho_i$  and  $U_i$  are the phase density and velocity, respectively, and  $A_{iw}$  is the area of contact between wall and phase for the current cell. The friction coefficient  $f_{iw}$  is calculated from the Blasius equation (Markatos and Singhal, 1982):

$$f_{iw} = 0.079 Re_i^{-0.25} \quad (15)$$

where the Reynolds number  $Re_i$  is based on the equivalent diameter of flow  $D_{eq}$  for the given cell. The quantities  $D_{eq}$  and  $A_{iw}$  depend on the flow regime, and the expressions used are given in Table 1 (Markatos and Singhal, 1982).

*Interphase friction* is calculated by the following linear expression (Markatos and Singhal, 1982):

$$F_{ip} = C_{fip} (U_g - U_l) \quad (16)$$

where  $C_{fip}$  is the interphase-friction coefficient, and is calculated differently for each flow regime.

In the present work, two expressions were used:

- Bubble and slug flow (Cheng et al., 1985):

$$C_{fip} = \frac{3}{8} 110.0 \rho_l |U_g - U_l| R_g (1.0 - R_g)^3 V_p \quad (17)$$

- Churn and annular flow (Govan et al., 1991):

$$C_{fip} = \frac{1}{2} f_{ip} \rho_g |U_g - U_l| \frac{4V_P R_g}{D \sqrt{R_g}} \quad (18)$$

where  $D$  is the equivalent diameter of flow for the two-phase mixture and  $f_{ip}$  is a friction factor given by the following relation (Govan et al., 1991):

$$f_{ip} = 0.005 + 14.44 R_l^{2.03} \quad (19)$$

It should be noted that no added mass terms are used in the model for simplicity. Bubbly flow is not desirable in airlift pumping, and is seldomly found because the bubbles quickly agglomerate and expand, yielding slug flow.

### **Pump simulation algorithm**

The objective when simulating an airlift pump is to determine the value of  $M_l$  (or  $M_g$ ), provided that  $M_g$  (or  $M_l$ ) is known. The simulation process of the whole system involves the coupling between flow in the suction pipe and the upriser. The pressure is calculated by the independent solution of the appropriate equations for the suction pipe and the upriser. A physically acceptable solution is obtained when these pressures are equal. This is the convergence criterion which stops the iteration procedure given below:

- a. A value for  $M_l$  (or  $M_g$ ) is estimated.
- b. The system of differential equations (6) to (9) describing the flow along the upriser together with Equations (10) and (11), and boundary conditions (12) and (13) is solved numerically for the estimated value of  $M_l$  (or  $M_g$ ). From this solution, the value of pressure at the injection point  $P_i$  is obtained.

- c. Equations (1) and (2) describing the flow in the suction pipe provide the pressure at the injection point  $P_i$ .
- d. If  $P_i$  from step b is equal to  $P_i$  as calculated in step c, the procedure has converged and the estimated value of  $M_l$  (or  $M_g$ ) is the solution. Otherwise, a new estimation for  $M_l$  (or  $M_g$ ) is made, and steps b through c are repeated until both values of  $P_i$  are practically the same.

Equations (6) to (9) are integrated over the volume of a cell enclosing a grid node. A conventional staggered grid (Patankar, 1980) was used, so that each velocity grid node is between two consecutive pressure cell nodes. Values of void fraction are calculated on the pressure grid nodes. Integration leads to a set of linearized finite-volume equations having the general form:

$$A_P \Phi_P = A_N \Phi_N + A_S \Phi_S + B \quad (20)$$

where  $\Phi$  is one of the dependent variables ( $U_g, U_b, R_g, R_l$ ),  $A, B$  are linear coefficients,  $N, S$  are the two neighbouring cells (North, South) of any arbitrary cell  $P$  (Figure 3). The pressure is calculated through a special pressure-correction equation based on Equation (10) (Spalding, 1981). The numerical solution procedure used is known as IPSA (InterPhase-Slip Algorithm). Further details may be found in references (Markatos, 1986, 1993; Markatos and Singhal, 1982; Spalding, 1981).

## Experimental data

A series of experiments were conducted by the Greek Institute of Geological and Mineral Exploration during the month of September 1988 in the Sidirokastro region of Xanthi, Northern Greece (Karydakis, 1988). The purpose of those experiments was to measure the liquid outflow of an inside airline pump for various lengths of internal pipe. An air compressor delivering 4.7 m<sup>3</sup>/min of air at 1 atm and 40°C was used at all times.

Seven sets of experiments are presented here. The experimental observations are shown in Tables 2 to 8 and are reported as volumetric water outflow  $V_l$  ( $\text{m}^3/\text{h}$ ) vs. airline length ( $L_d + L_s$ ) of the upriser pipe and water level ( $L_s + L_e$ ). The latter is defined as the length of the submerged outer pipe (see also Figure 1). The first three sets of experiments (Tables 2 to 4) correspond to one group where the total length  $L$  of the pipe and its outer diameter  $D$  are kept constant, while the inner diameter  $d$  is changed. The water temperature was at  $56^\circ\text{C}$ . The second group of experimental observations is given in Tables 5 to 7, for a shorter total length  $L$  and a cooler water temperature of  $42^\circ\text{C}$ . Finally, Table 8 presents experimental observations for a much shorter pipe length  $L$  (about half the previous lengths).

## Results and discussion

Simulations have been carried out for the seven sets of experiments reported above (Tables 2 to 8) by using both the simple *mean air-volume fraction model* (see appendix) and the *hydrodynamic model* presented above. First, we have established the adequacy of the number of cells in the finite-volume grid to obtain results independent of its density. A grid of 50 cells along the upriser was used to solve the differential equations. The adequacy of using this number of cells is manifested in Figure 5, where the air-volume fraction  $R_g$  along the upriser becomes practically grid-independent for the 25- and 50-cell solutions.

The results from the simulations corresponding to the experimental observations given in Tables 2 to 8 are shown in Figures 6 to 12, respectively. In each figure we plot the volumetric flow rate  $V_l$  of the water outflow as a function of the airline length  $L_u=(L_d + L_s)$  of the upriser pipe. It is seen that in most cases, the mean air-volume fraction model gave unrealistic predictions. On the other hand, the hydrodynamic model simulates all cases rather well. In particular, simulations for the

sets of experiments 2, 3, 5, 6 and 7 were more accurate than those for series 1 and 4. The less accurate predictions of the hydrodynamic model for series 1 and 4 is caused by the poor response of the correlations used to calculate the interphase friction term in Equation (16). The correlations give poor results in the slug and churn flow regimes (Taitel et al., 1980; Cheng et al., 1985) (where the air-volume fraction ranges from about 0.3 to 0.6). This is elucidated in Figures 6 and 13 (corresponding to the first set of experiments of Table 2), where predictions improve as the flow pattern along the upriser is increasingly dominated by the annular regime.

The deviations between simulation and experiment are shown in Figures 14 and 15. Those diagrams show that the mean air-volume fraction model is clearly out of the 30% error region with an overestimation (positive error) tendency, while the hydrodynamic model is inside the 30% region, without any particular over- or under-estimation tendency.

Finally, for each set of experiments the mean error and the standard deviation were examined. The mean error is defined by the following expression:

$$\text{Mean \% error} = \frac{\sum \left| \frac{M_{l,\text{predicted}} - M_{l,\text{experimental}}}{M_{l,\text{experimental}}} \right|}{\text{Number of observations}} \times 100\% \quad (21)$$

Error results are shown in Table 9. Besides sufficient accuracy, the predictions demonstrate a small standard deviation, meaning that the experimental curve was simulated realistically (without "jumps", oscillations or other types of non-physical behaviour). On the other hand, the predictions obtained by the mean air-volume fraction model were very unsatisfactory, yielding errors as high as 136%, while the present model gave at worst an error of 29%.

## Conclusions

In this work, a differential, two-phase hydrodynamic model was presented for the simulation of airlift pumps. Predictions were obtained both by the hydrodynamic model and a mean air-volume fraction model, and compared with real field experimental data. Both models predicted correctly the overall behavioural trend of the experiments. However, it was shown that the predictions based on the hydrodynamic model were, in all cases, significantly better in comparison to the mean void fraction model. This is because the hydrodynamic model takes into account the gas compressibility itself (in the momentum and continuity equations) and all the effects that result from this (i.e., multiple flow regimes). The mean air-volume fraction model might give better predictions if a single flow regime were predominant along the upriser. However, for water wells of moderate to large depths, the compressibility effects of the gas phase are large, which among other things, leads to multiple flow regimes.

Differential equation models are economical and versatile. At the same time they generally give more reliable results than empirical correlations. Accurate predictions can be developed only when the interphase velocity slip  $|U_g - U_l|$  is accurately estimated. This, in turn, is determined by the interphase friction factor  $C_{fp}$ . As far as the effect of friction coefficients is concerned, frictional terms in vertical flows are not the dominating terms in the governing differential equations, so great accuracy in friction correlations does not affect the results very much. Results can be improved when better correlations are used for the churn flow regime.

Better results can also be achieved by implementing a two-dimensional approach, especially for internal airline systems due to their geometry.

It is possible and relatively easy to extend the present model for solving more complex problems, such as optimization of air compressors, pipe diameters, simulation of tapered pipe systems, determination of optimum flow conditions or behaviour for fluctuating demand.

## **Acknowledgments**

Financial assistance from the Natural Sciences and Engineering Research Council (NSERC) of Canada for one of the authors (E. Mitsoulis) is gratefully acknowledged. The authors would also like to thank the Greek Institute of Geological and Mineral Exploration (IGME) for providing the experimental data.

## Appendix - Mean air-volume fraction model

Kato et al. (1975) proposed a simple model for airlift simulation, based on the momentum balance along the upriser. According to their work, the water flow rate ( $M_l$ ) or required air injection rate ( $M_g$ ) can be estimated by solving the following equation:

$$\frac{2V_l^2 f_{mix}}{gL} \left[ \frac{L_e}{D_1 A_1^2} + \frac{L_s + L_d}{D_2 A_2^2} (1 - \bar{R}_g)^{-1.75} + \frac{1}{2} \left( \frac{1}{1 - \bar{R}_g} - \frac{3}{4} \right) \right] + \frac{L_d}{L_d + L_s} - \bar{R}_g = 0 \quad (A1)$$

where  $V_l$  is the volumetric flow rate of the liquid phase,  $f_{mix}$  is the friction coefficient of the mixture,  $g$  is gravity,  $L$  is the total length of the pipe,  $D$  is the pipe diameter,  $A$  is the cross-sectional pipe area and  $\bar{R}_g$  is the mean air-volume fraction along the upriser. The latter is calculated by the Zuber-Findlay (1965) correlation:

$$\bar{R}_g = \frac{\bar{V}_g}{\bar{V}_g + V_l + 0.35 A_2 \sqrt{g D_2}} \quad (A2)$$

where  $\bar{V}_g$  is the mean air-volumetric flow along the upriser, calculated by assuming isothermal expansion between points 1 and 2 (see Figure 1):

$$\bar{V}_g = V_{g,2} \left( \frac{P_2}{P_1 - P_2} \right) \ln \frac{P_1}{P_2} \quad (A3)$$

The air injection pressure  $P_i$  is calculated by applying the Bernoulli equation between points 1 and  $i$  (Figure 1). Other parameters needed in Equation (A1) are given below (Kato et al., 1975):

$$f_{mix} = 0.079 \text{Re}_{mix}^{-0.25} \quad (A4)$$

$$\text{Re}_{mix} = \frac{M_l + M_g}{A_2 \mu_l} D_2 \quad (\text{A5})$$

where  $\text{Re}_{mix}$  is the mixture Reynolds number in the upriser pipe.

## Nomenclature

A	= linear coefficient of finite-volume Equation (20)
$A_1$	= cross section of suction pipe (one-phase flow), $\text{m}^2$
$A_2$	= cross section of upriser (two-phase flow), $\text{m}^2$
$A_{iw}$	= area of contact between wall and phase, $\text{m}^2$
B	= linear coefficient of finite-volume Equation (20)
C	= interphase friction coefficient, dimensionless
d	= diameter of airline pipe, m
D	= diameter of outer pipe, m
$D_1$	= equivalent diameter of suction pipe, m
$D_2$	= equivalent diameter of upriser, m
$f^{ij}$	= volumetric friction force term in the momentum equation, $\text{N}/\text{m}^3$
$f_{ij}$	= friction coefficient, dimensionless
F	= frictional force, N

$g$	= gravity acceleration, $\text{m/s}^2$
$L$	= length of outer pipe: $L_s+L_d+L_e$ , m
$L_d$	= length of discharge above water level, m
$L_e$	= length of suction pipe, m
$L_s$	= length of discharge below water level, m
$M$	= mass flow rate, $\text{kg/s}$
$NC$	= number of computational cells in the upriser
$P$	= pressure, Pa
$R$	= volume fraction, dimensionless
$Re$	= Reynolds number, $Re=\rho UD/\mu$ , dimensionless
$t$	= time, s
$T$	= temperature, $^{\circ}\text{C}$
$U$	= velocity, $\text{m/s}$
$U_{gs}, U_{ls}$	= superficial gas and liquid velocity: $V_i/A_2$ , $i=g,l$ , $\text{m/s}$
$V$	= volumetric flow rate, $\text{m}^3/\text{s}$
$V_p$	= volume of a computational cell, $\text{m}^3$
$z$	= axial distance, m

***Greek letters***

$\Delta z$	= distance, $(L_s+L_d)/NC$ , m
$\mu$	= viscosity, Pa·s
$\xi$	= entry loss factor, dimensionless
$\rho$	= density, $\text{kg/m}^3$
$\ddot{O}$	= dependent variable

***Subscripts***

1, 2, i	= value at position 1, 2, i
eq	= equivalent
fip	= interphase friction
g	= gas phase
ip	= interphase
iw	= wall-phase i (gas or liquid)
k	= value of a property at cell node k
l	= liquid phase
mix	= mixture
N	= north cell

P = scalar variable cell

S = south cell

w = well

z = flow direction

### *Superscripts*

gl = gas-liquid

gw = gas-wall

iw = wall-phase i (gas or liquid)

lg = liquid-gas

lw = liquid-wall

— = mean value

## References

- Casey, T.J., "Water and Wastewater Engineering", Oxford University Press, Oxford (1992), p. 181.
- Cheng, L.Y., D.A. Drew and R.T. Lahey Jr., "An Analysis of Wave Propagation in Bubbly-Two-Component, Two-Phase Flow", Trans. ASME, J. Heat Transfer **107**, 402-408 (1985).
- Chisti, Y., "Assure Bioreactor Sterility", Chem. Eng. Prog., 88(9), p. 80 (September 1992).
- Gibson, A.H., "Hydraulics and its Applications", 5th ed., Constable, London (1961).
- Giot, M., "Three Phase Flow", in "Handbook of Multiphase Systems", G. Hetsroni, ed., Hemisphere-McGraw Hill, Washington, DC (1982), p. 7.29.
- Govan, A.H., G.F. Hewitt, H.J. Richter and A. Scott, "Flooding and Churn Flow in Vertical Pipes", Int. J. Multiphase Flow **17**, 27-44 (1991).
- Hjalmar, S., "The Origin of Instability in Airlift Pumps", Trans. ASME, J. Appl. Mech. **40**, 399-404 (1973).
- Karydakis, G., "Experimental Data of Airlift Pump Systems", Internal Report, Institute of Geological and Mineral Exploration, Athens (1988).
- Kato, H., T. Miyazawa, S. Timaya and T. Iwasaki, "A Study of an Airlift Pump for Solid Particles", Bull. JSME **18**, 286-294 (1975).
- Markatos, N.C., "Modelling of Two-Phase Transient Flow and Combustion of Granular Propellants", Int. J. Multiphase Flow **12**, 913-933 (1986).

- Markatos, N.C., "Mathematical Modelling of Single and Two-Phase Flow Problems in the Process Industries", *Rev. Inst. Franç. Petr.* **48**, 631-662 (1993).
- Markatos, N.C. and A.K. Singhal, "Numerical Analysis of One-Dimensional, Two-Phase Flow in a Vertical Cylindrical Passage", *Adv. Eng. Software* **4**, 99-106 (1982).
- Mero, J.L., "Seafloor Minerals: A Chemical Engineering Challenge", *Chem. Eng.*, 43(2), p. 73 (1968).
- Patankar, S.V., "Numerical Heat Transfer and Fluid Flow", McGraw-Hill, New York (1980).
- Spalding, D.B., "Mathematical Methods in Nuclear Reactor Thermal Hydraulics", CHAM HTS/81/3 (1981).
- Taitel, Y., D. Bornea and A.E. Buckler, "Modelling Flow Pattern Transitions for Steady Upward Gas-Liquid Flow in Vertical Tubes", *AIChE J.* **26**, 345-354 (1980).
- Trystam, G. and S. Pigache, "Modelling and Simulation of a Large Scale Air Lift Fermenter", in "Proc. Eur. Symp. Comp.-Aid. Proc. Eng.-2" (1992), pp. 5171-5176.
- Wallis, G.B., "One-Dimensional Two-Phase Flow", McGraw-Hill, New York (1969).
- Zenz, F.A., "Explore the Potential of Air-Lift Pumps and Multiphase Systems", *Chem. Eng. Prog.*, 89(8), p. 51 (August 1993).
- Zuber, N. and J.A. Findlay, "Average Volumetric Concentration in Two-Phase Flow Systems", *ASME J. Heat Transfer* **87**, 453-468 (1965).

TABLE 1

Contact Area and Equivalent Diameter of Flow for Different Flow Regimes (Markatos and Singhal, 1982)

Flow Regime	$A_{l,w}$	$A_{g,w}$	$D_l$	$D_g$
Bubble, Slug	$\left(\frac{4V_P}{D}\right)R_l D$	$\left(\frac{4V_P}{D}\right)R_g E$	D	D
Churn, Annular	$\frac{4V_P}{D} F$	0	$DR_l G$	$D\sqrt{R_g} H$

TABLE 2

First Set of Measurements,  $L=46.6$  m,  $D=10.16$  cm,  $d=2.54$  cm, Water Temperature  $T_w=56^\circ\text{C}$  (Karydakis, 1988)

Obs'n No.	Airline Length (m) $L_d + L_s$	Water Level (m) $L_s + L_e$	Water Outflow ( $\text{m}^3/\text{h}$ )
1	45.80	22.70	25.5
2	42.20	22.90	23.0
3	39.20	23.10	19.0
4	36.20	23.20	16.0
5	33.20	23.40	11.0
6	30.20	23.50	6.0

TABLE 3

Second Set of Measurements,  $L=46.6$  m,  $D=10.16$  cm,  $d=1.91$  cm, Water Temperature  $T_w=56^\circ\text{C}$  (Karydakis, 1988)

Obs'n No.	Airline Length (m) $L_d + L_s$	Water Level (m) $L_s + L_e$	Water Outflow ( $\text{m}^3/\text{h}$ )
1	46.20	22.80	27.0
2	42.20	22.90	23.0
3	39.20	23.20	20.0
4	36.20	23.40	16.0
5	33.20	23.50	11.0
6	30.20	23.60	5.0

TABLE 4

Third Set of Measurements,  $L=46.6$  m,  $D=10.16$  cm,  $d=1.27$  cm, Water Temperature  $T_w=56^\circ\text{C}$  (Karydakis, 1988)

Obs'n No.	Airline Length (m) $L_d + L_s$	Water Level (m) $L_s + L_e$	Water Outflow ( $\text{m}^3/\text{h}$ )
1	36.20	23.40	13.6
2	33.20	23.50	8.2
3	30.20	23.50	4.0

TABLE 5

Fourth Set of Measurements,  $L=45.1$  m,  $D=10.16$  cm,  $d=1.27$  cm, Water Temperature  $T_w=42^\circ\text{C}$  (Karydakis, 1988)

Obs'n No.	Airline Length (m) $L_d + L_s$	Water Level (m) $L_s + L_e$	Water Outflow ( $\text{m}^3/\text{h}$ )
1	24.20	40.10	42.0
2	18.20	40.20	34.0
3	12.20	40.50	22.0

TABLE 6

Fifth Set of Measurements,  $L=45.1$  m,  $D=10.16$  cm,  $d=1.91$  cm, Water Temperature  $T_w=42^\circ\text{C}$  (Karydakis, 1988)

Obs' nNo.	Airline Length (m) $L_d + L_s$	Water Level (m) $L_s + L_e$	Water Outflow ( $\text{m}^3/\text{h}$ )
1	30.20	39.87	48.0
2	24.20	40.18	40.0
3	18.20	40.22	33.0
4	12.20	40.45	22.0

TABLE 7

Sixth Set of Measurements,  $L=45.1$  m,  $D=10.16$  cm,  $d=2.54$  cm, Water Temperature  $T_w=42^\circ\text{C}$  (Karydakis, 1988)

Obs'n No.	Airline Length (m) $L_d + L_s$	Water Level (m) $L_s + L_e$	Water Outflow ( $\text{m}^3/\text{h}$ )
1	30.20	39.20	43.5
2	24.20	39.70	38.0
3	18.20	39.80	31.0
4	12.20	40.20	19.0

TABLE 8

Seventh Set of Measurements,  $L=24.3$  m,  $D=7.62$  cm,  $d=1.27$  cm, Water Temperature  $T_w=42^\circ\text{C}$  (Karydakis, 1988)

Obs'n No.	Airline Length (m) $L_d + L_s$	Water Level (m) $L_s + L_e$	Water Outflow ( $\text{m}^3/\text{h}$ )
1	24.10	11.30	9.4
2	23.30	11.40	8.4
3	22.80	11.40	8.2
4	21.80	11.50	7.4
5	20.30	11.70	5.5

TABLE 9

Comparison of Both Models: Mean (%) Error and Standard Deviation (in Parentheses)

Experimental Series	Mean Air-Volume Fraction Model	Hydrodynamic Model
1	29.6 (9.3)	17.5 (7.7)
2	51.9 (2.8)	8.2 (6.5)
3	136.2 (4.7)	25.5 (11.2)
4	66.1 (10.2)	29.0 (8.6)
5	49.2 (4.5)	7.8 (4.5)
6	43.1 (3.6)	4.8 (4.1)
7	47.2 (2.5)	7.3 (1.8)

## List of figures

- Figure 1 : Schematic representation of an airlift pumping system.
- Figure 2 : Schematic representation of external and internal airline pumping systems.
- Figure 3 : Definition of cells along the upriser pipe for the finite-volume method of computation.
- Figure 4 : Example of a flow regime map (Taitel et al., 1980).
- Figure 5 : Grid independence of the simulation results (air-volume fraction along the upriser).
- Figure 6 : Volumetric water outflow vs. airline length of the upriser pipe for the first data series (see Table 2) - comparison of models with experiment.
- Figure 7 : Volumetric water outflow vs. airline length of the upriser pipe for the second data series (see Table 3) - comparison of models with experiment.
- Figure 8 : Volumetric water outflow vs. airline length of the upriser pipe for the third data series (see Table 4) - comparison of models with experiment.
- Figure 9 : Volumetric water outflow vs. airline length of the upriser pipe for the fourth data series (see Table 5) - comparison of models with experiment.
- Figure 10: Volumetric water outflow vs. airline length of the upriser pipe for the fifth data series (see Table 6) - comparison of models with experiment.
- Figure 11: Volumetric water outflow vs. airline length of the upriser pipe for the sixth data series (see Table 7) - comparison of models with experiment.
- Figure 12: Volumetric water outflow vs. airline length of the upriser pipe for the seventh data series (see Table 8) - comparison of models with experiment.
- Figure 13: Predicted flow regimes along the upriser pipe for the first data series (see Table 2 and Figure 6). Note that observation No. 1 corresponds to the highest length and water outflow and observation No. 6 to the lowest values.

Figure 14: Deviation between experimental and mean air-volume fraction model predictions for volumetric water outflow ( $\text{m}^3/\text{h}$ ).

Figure 15: Deviation between experimental and hydrodynamic model predictions for volumetric water outflow ( $\text{m}^3/\text{h}$ ).

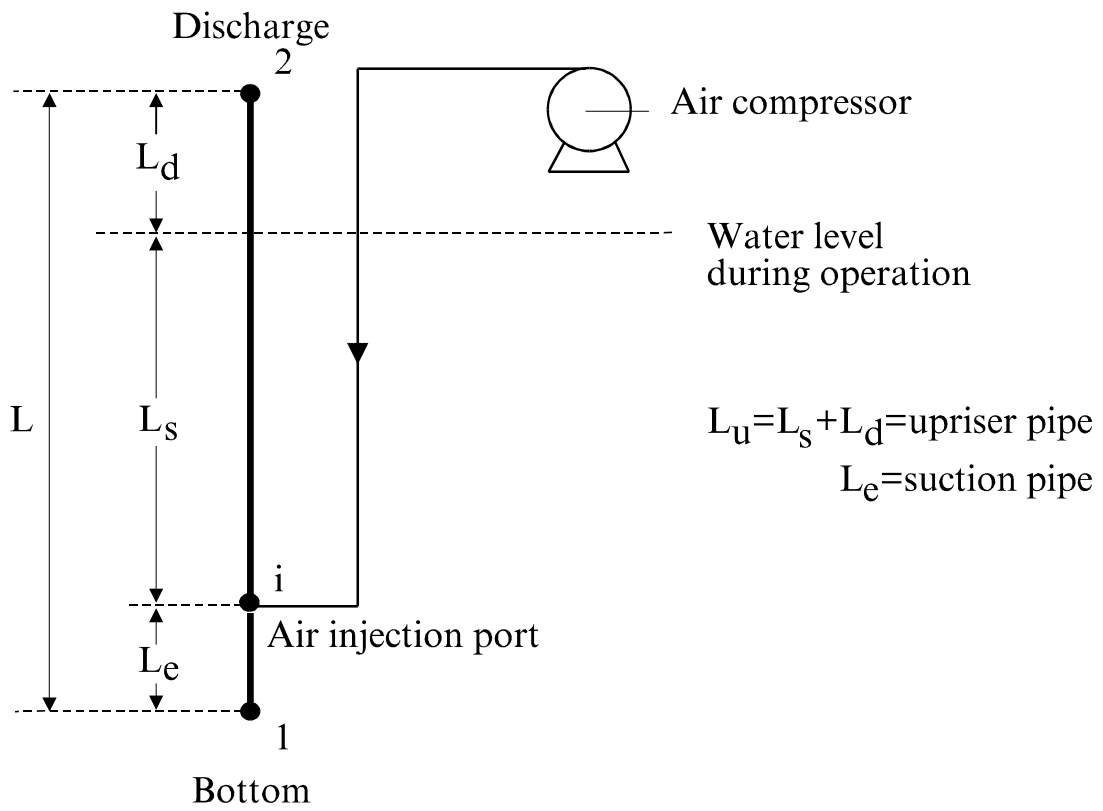


Figure 1

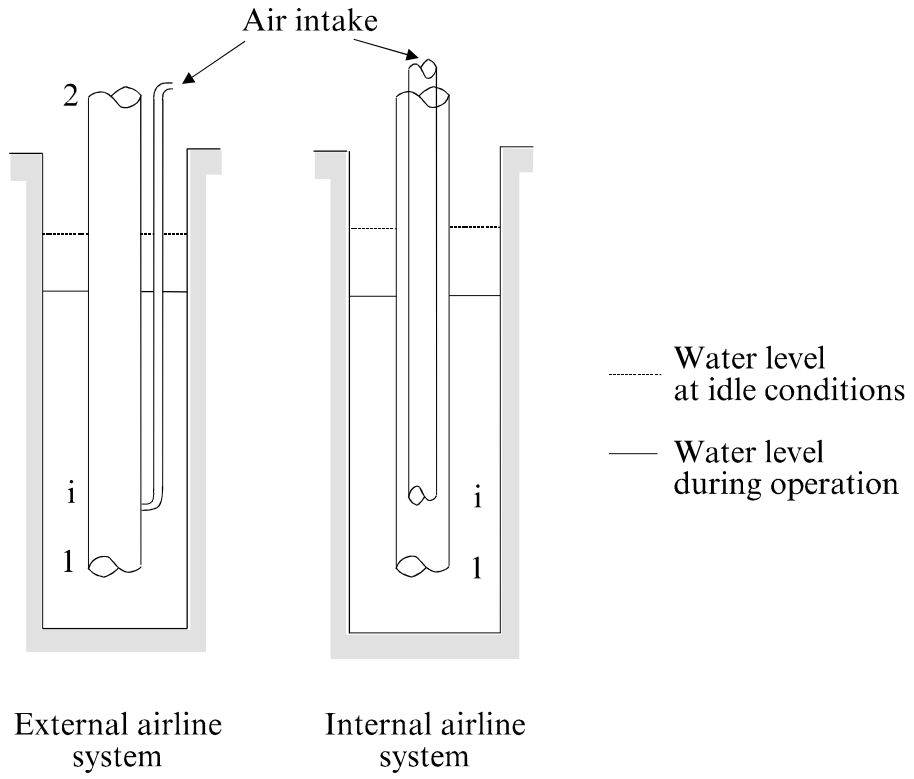


Figure 2

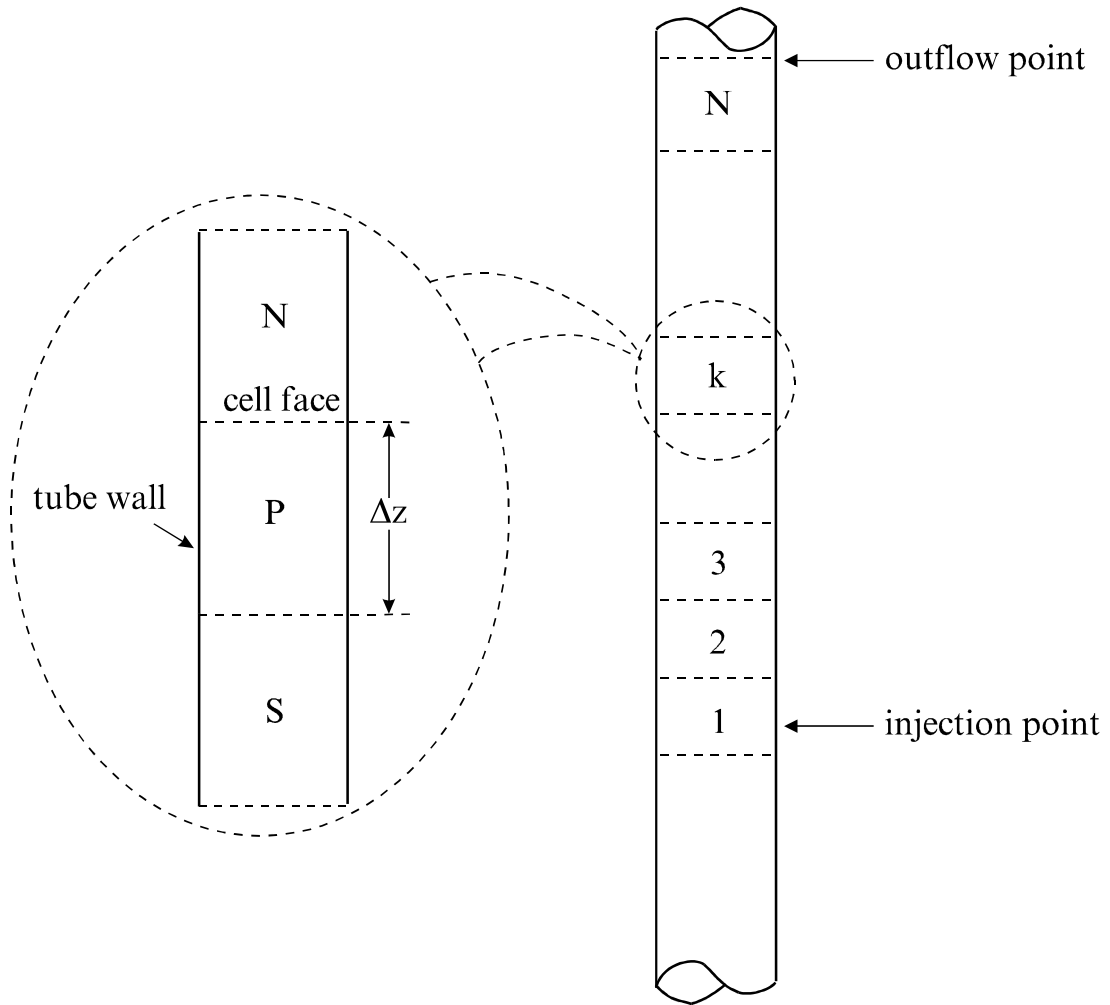


Figure 3

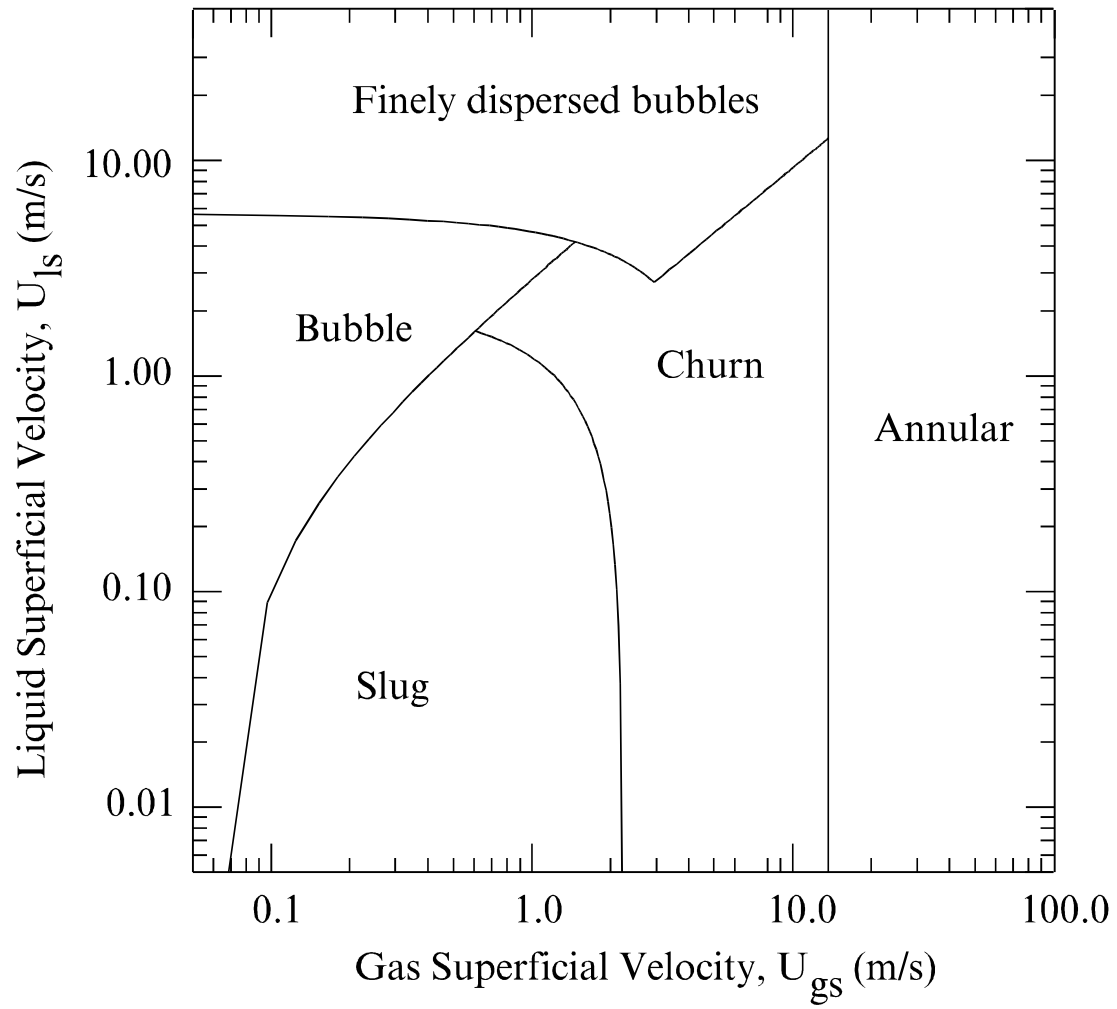


Figure 4

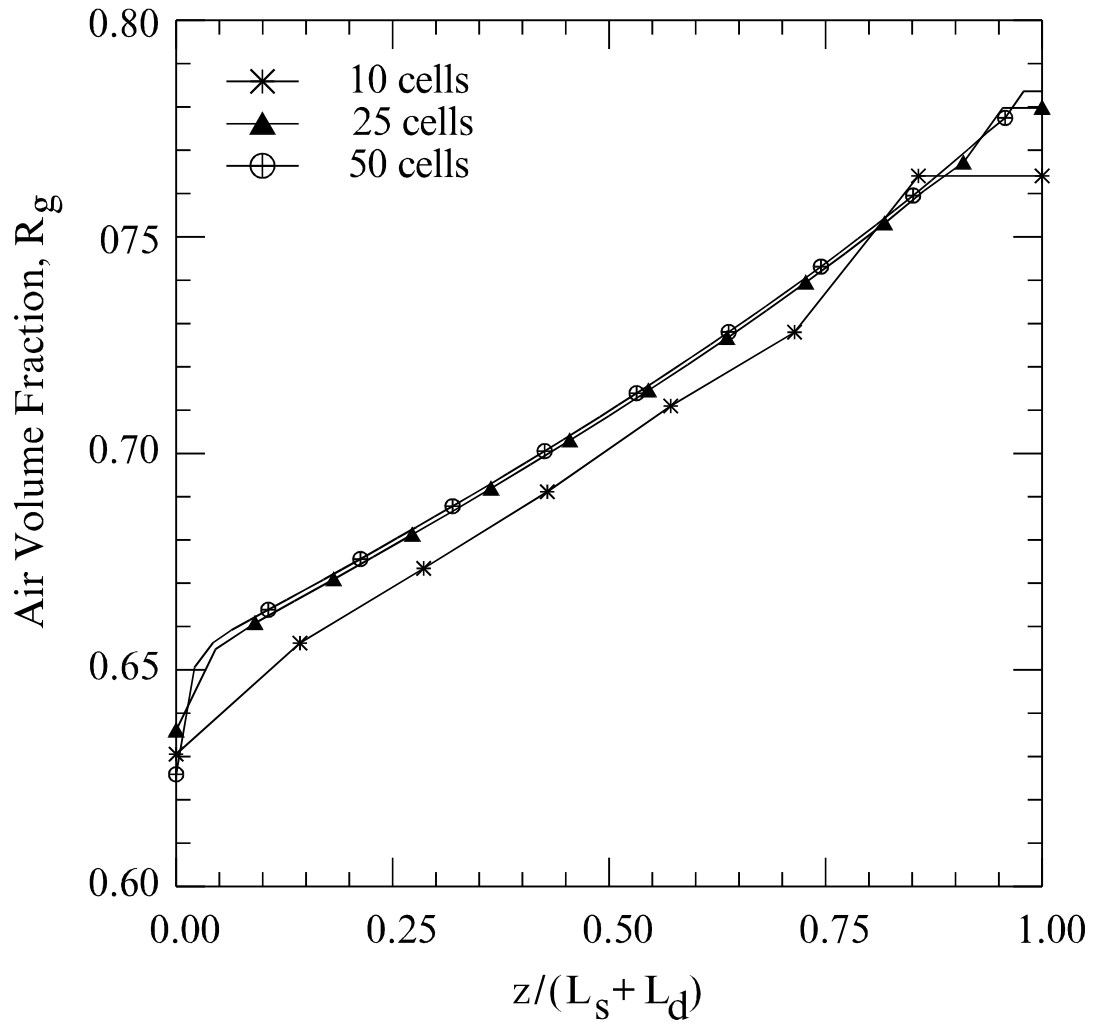


Figure 5

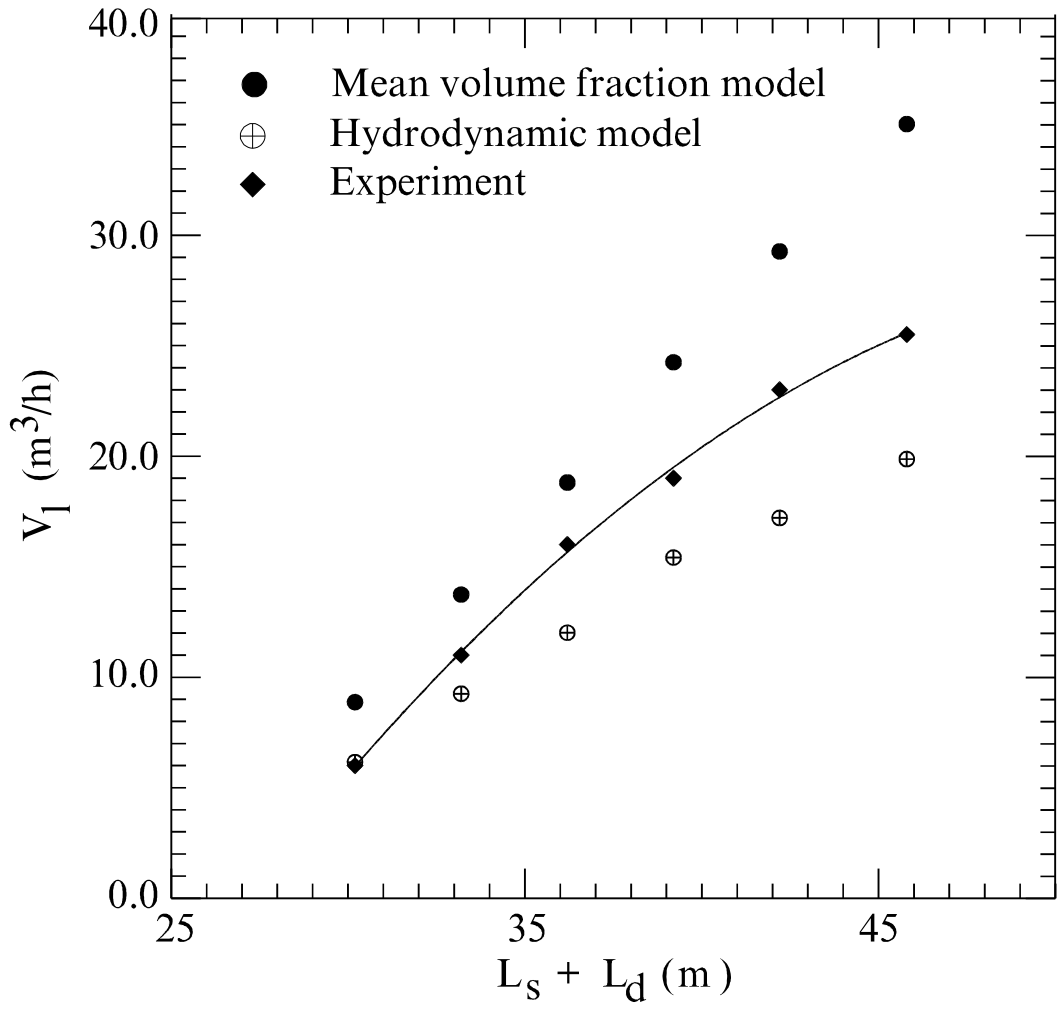


Figure 6

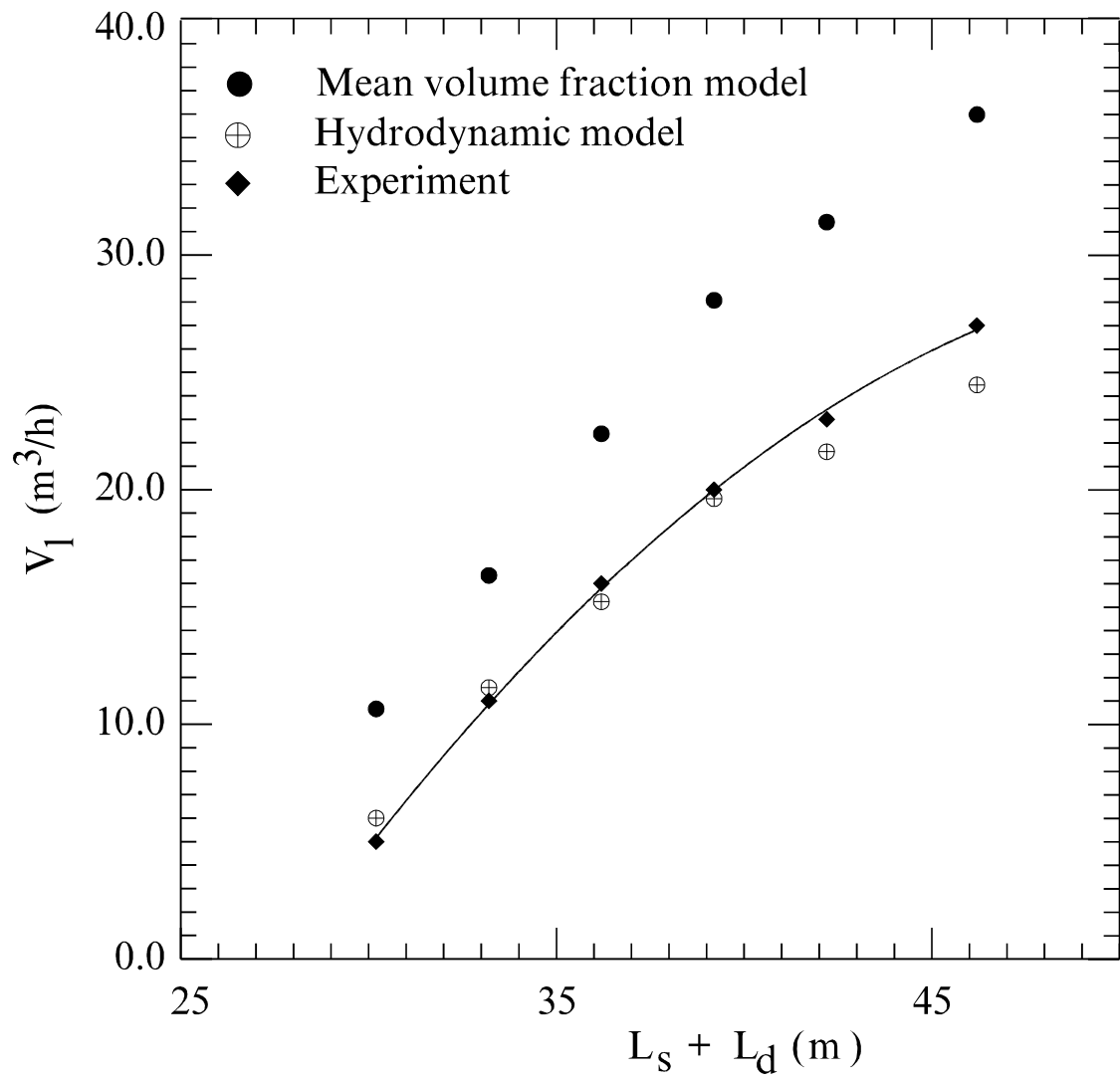


Figure 7

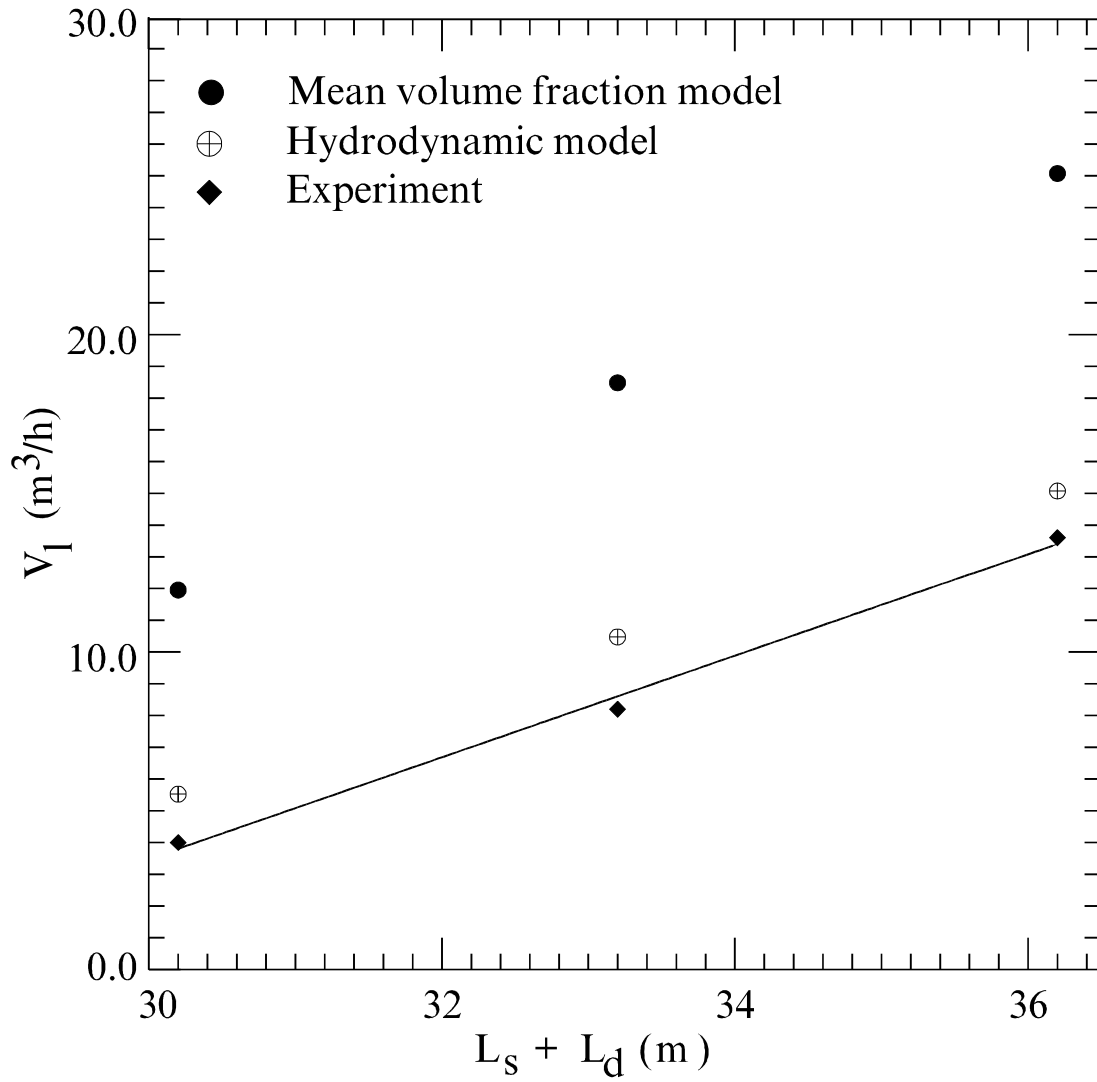


Figure 8

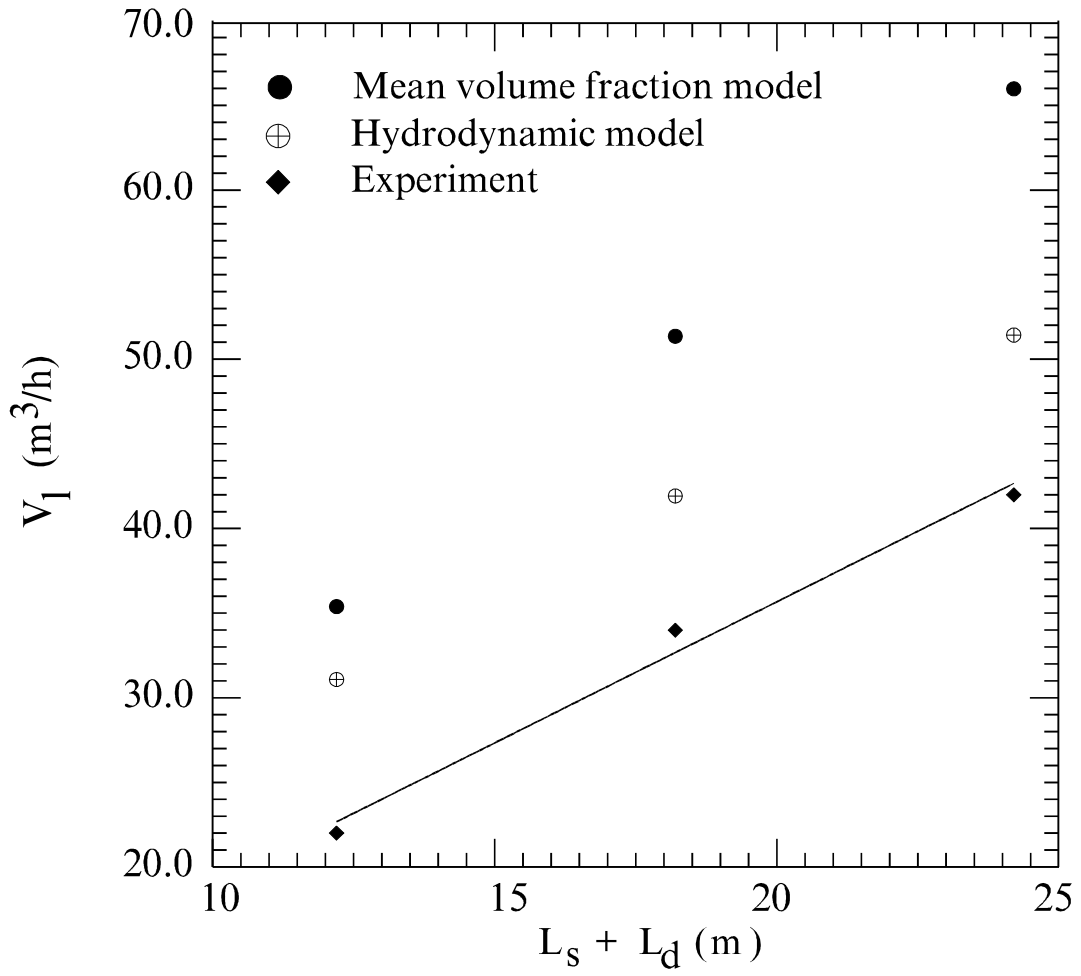


Figure 9

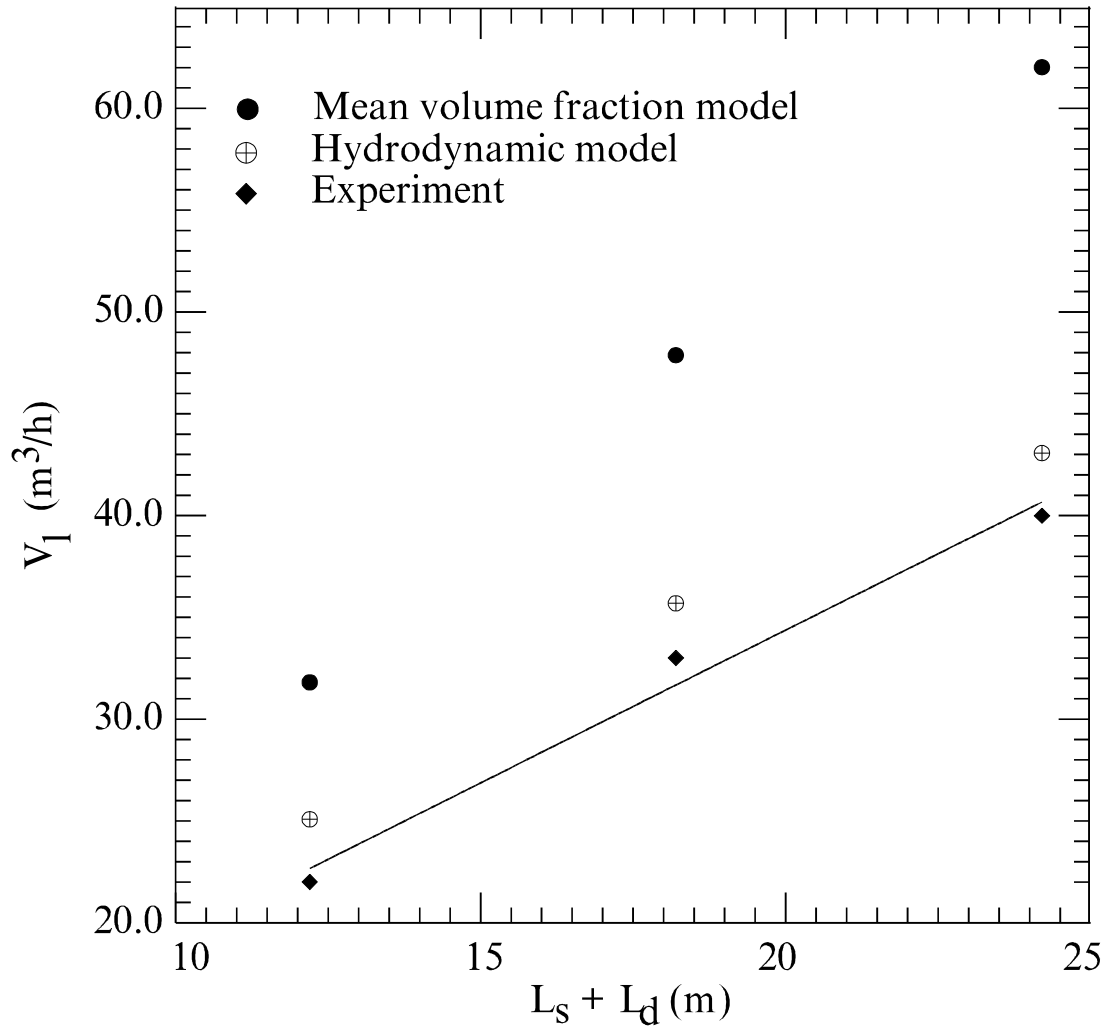


Figure 10

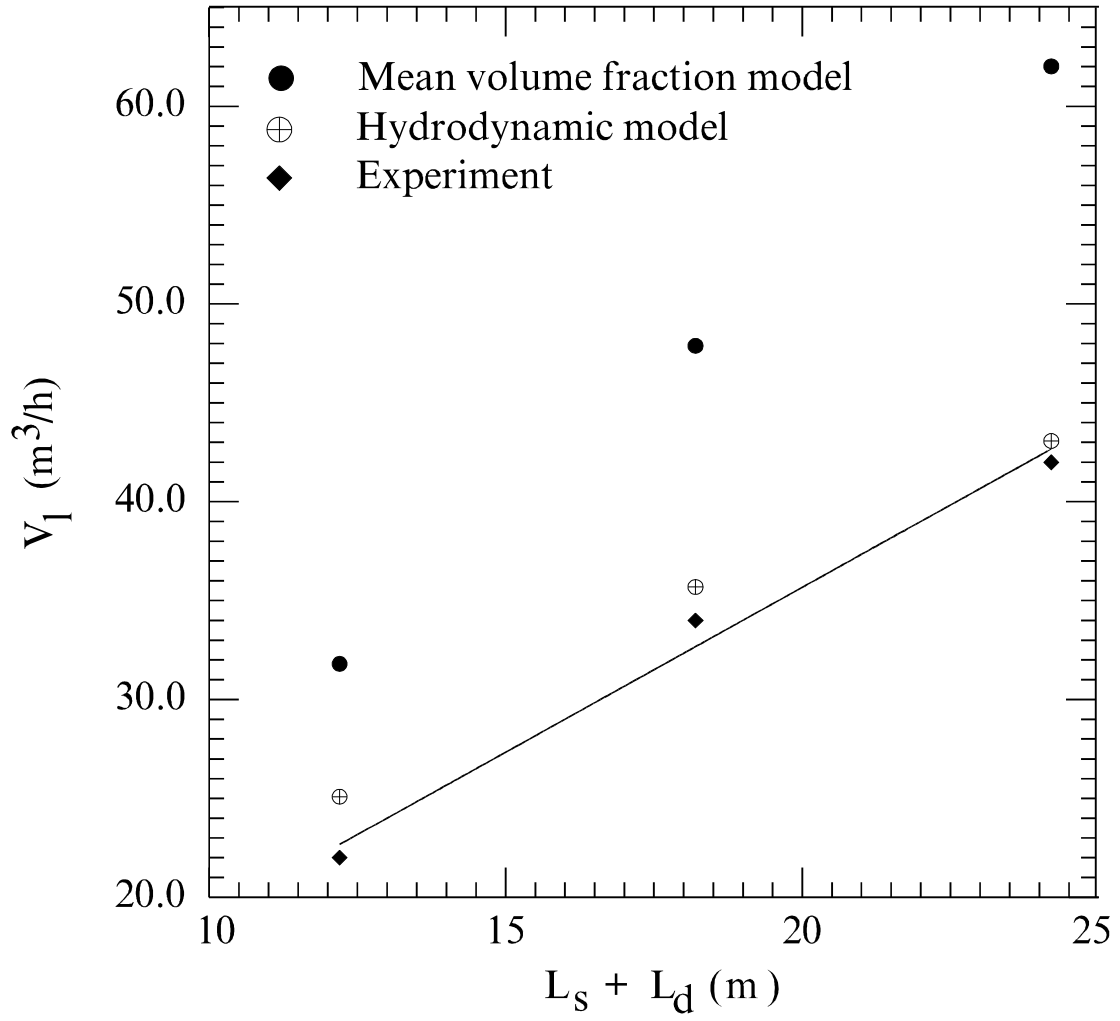


Figure 11

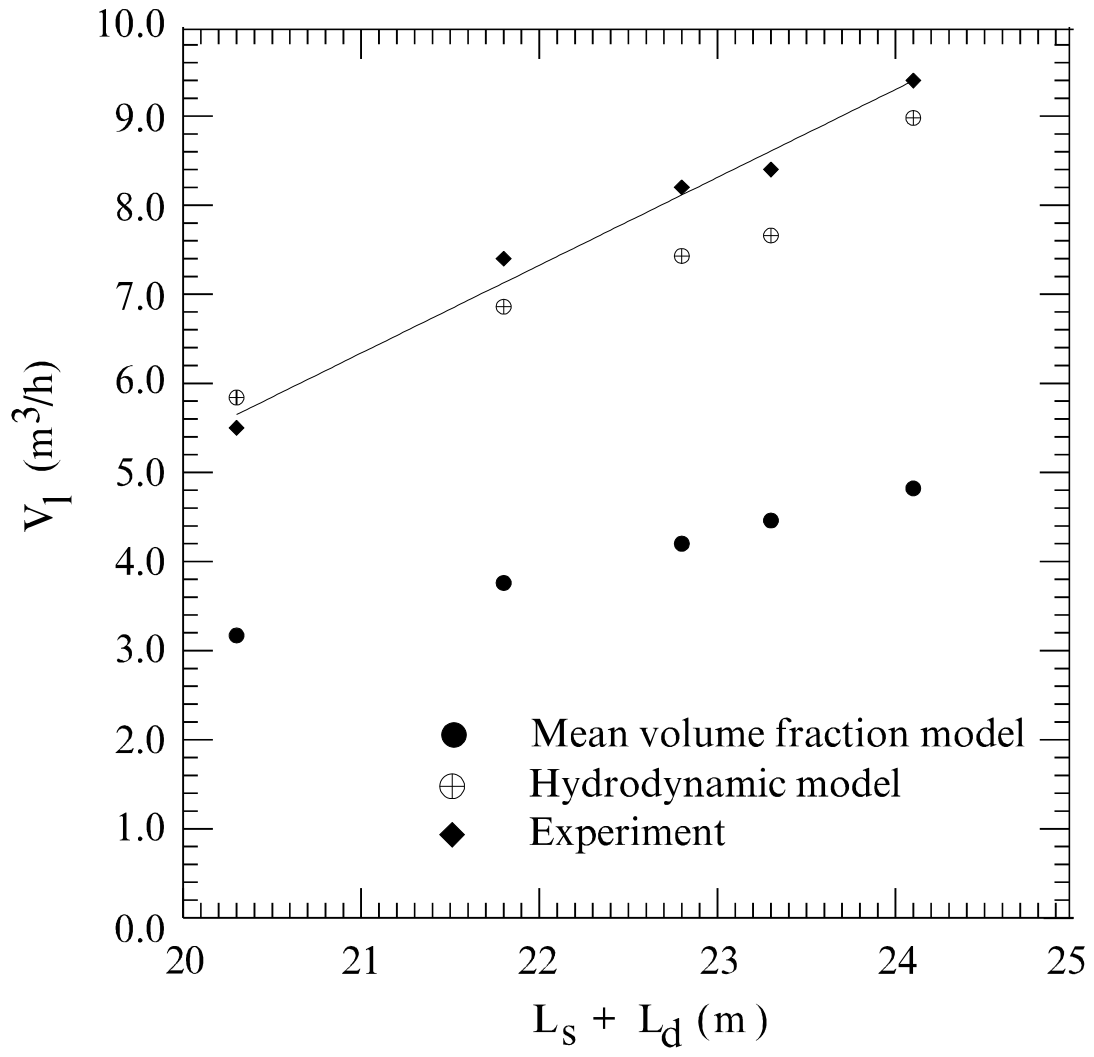


Figure 12

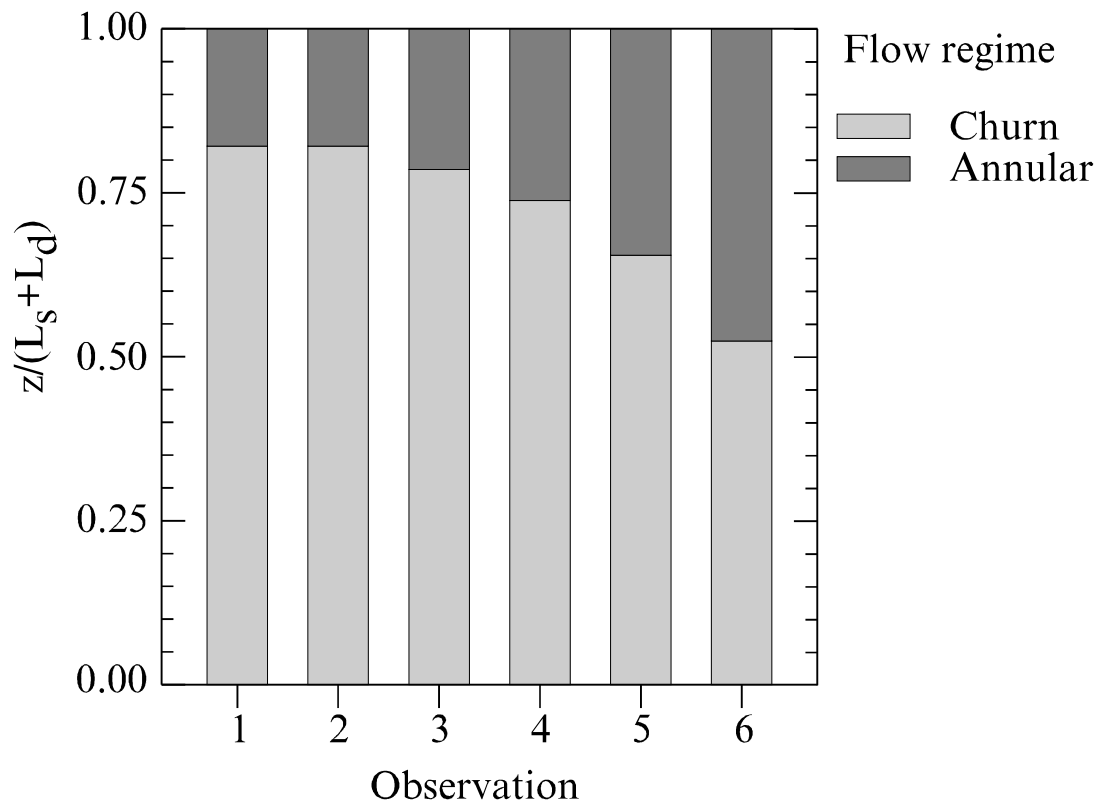


Figure 13

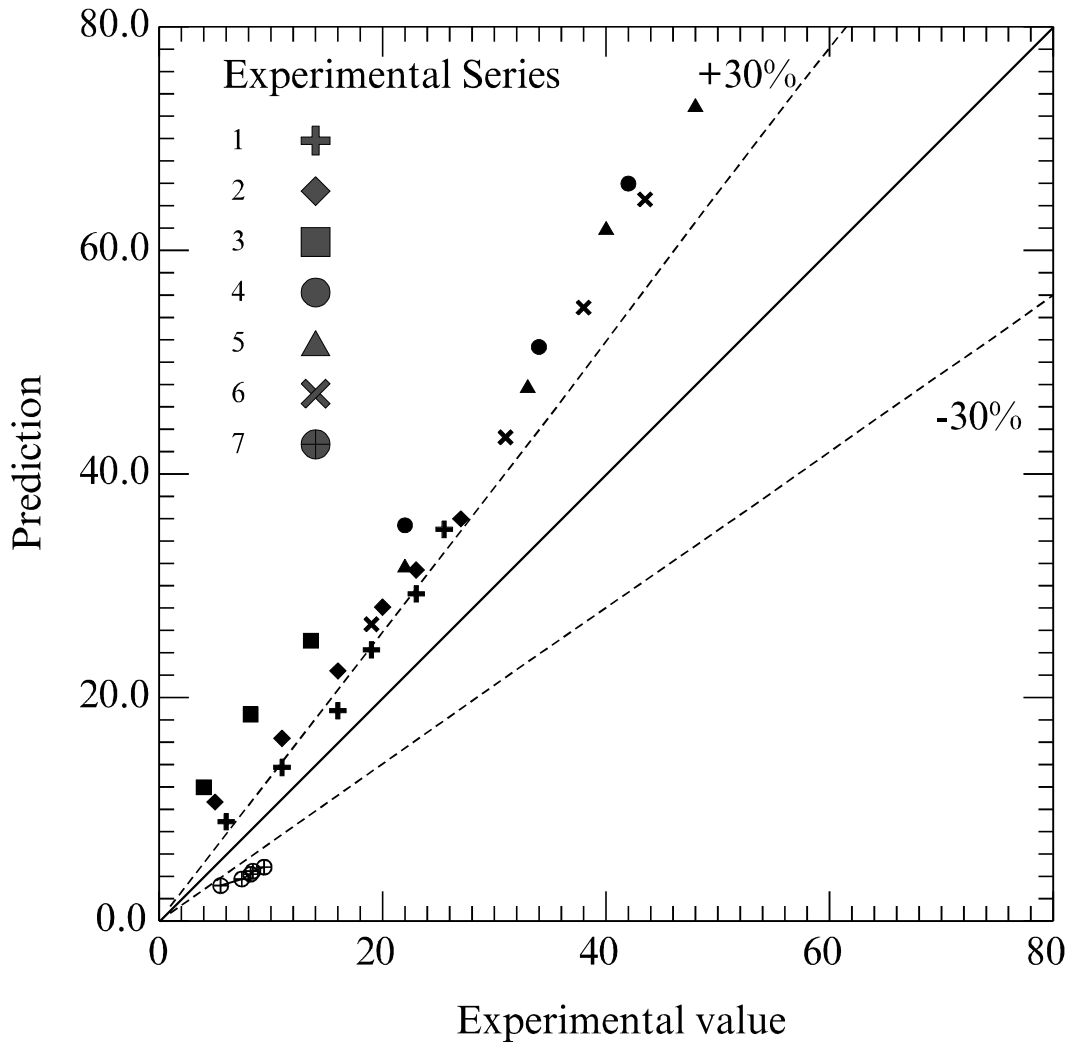


Figure 14

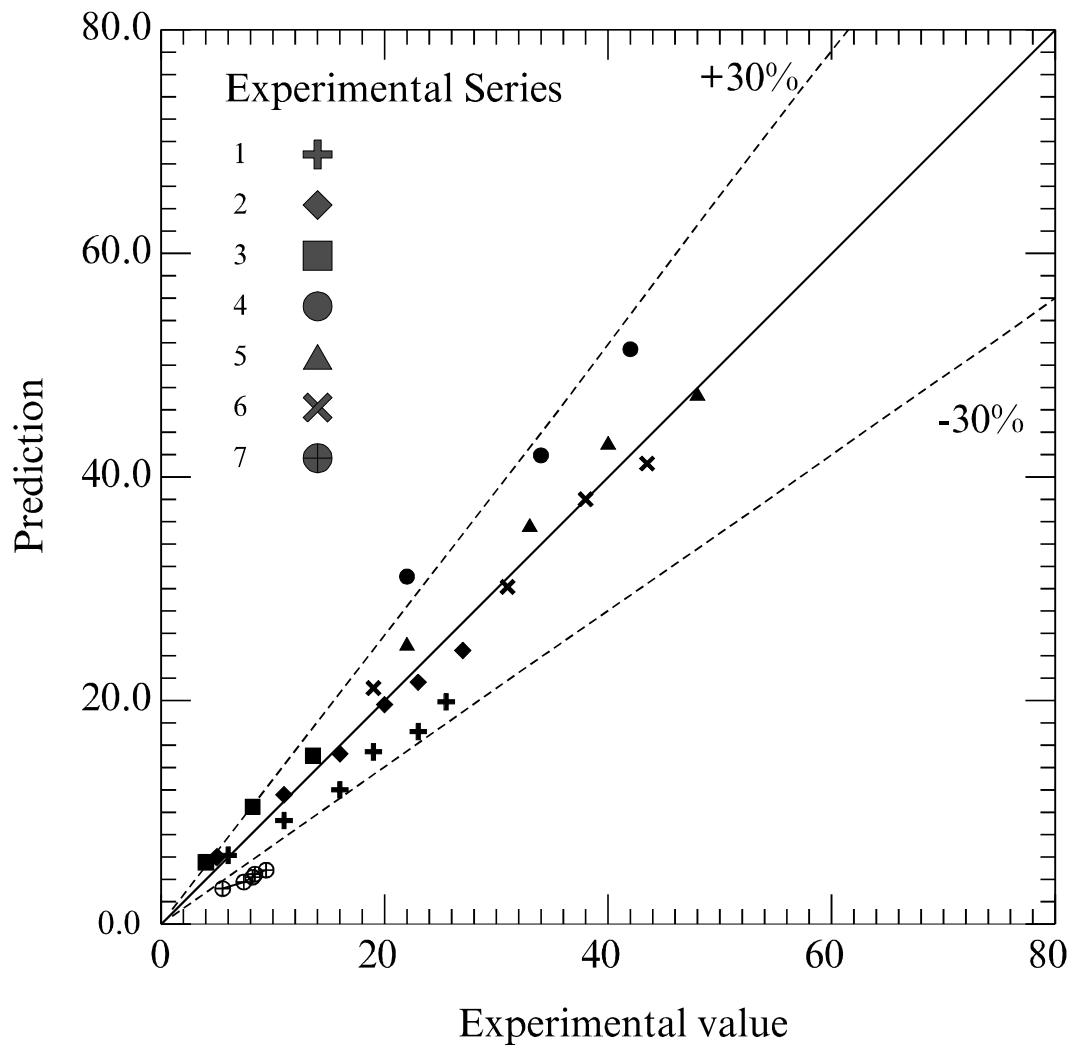


Figure 15